Supplemental Information for: Spin Vortex Crystal Order in Organic Triangular Lattice Compound

Kira Riedl,[1] Elena Gati,[2,3] David Zielke,[2] Steffi Hartmann,[2] Oleg M. Vyaselev,[4] Nataliya D. Kushch,[5] Harald O. Jeschke,[6] Michael Lang,[2] Roser Valentí,[1] Mark V. Kartsovnik,[7] and Stephen M. Winter*[8]

[1] *Institut für Theoretische Physik, Goethe-Universität Frankfurt, Max-von-Laue-Strasse 1, 60438 Frankfurt am Main, Germany*
[2] *Physikalisches Institut, Goethe-Universität Frankfurt, Max von Laue Str 1, 60438 Frankfurt am Main, Germany*
[3] *Max Planck Institute for Chemical Physics of Solids, Dresden, Germany*
[4] *Institute of Solid State Physics, Russian Academy of Sciences, 142432 Chernogolovka, Russia*
[5] *Institute of Problems of Chemical Physics, Russian Academy of Sciences, 142432 Chernogolovka, Russia*
[6] *Research Institute for Interdisciplinary Science, Okayama University, Okayama 700-8530, Japan*
[7] *Walther-Meissner-Institut, Bayerische Akademie der Wissenschaften, Walther-Meissner-Strasse 8, Garching D-85748, Germany*
[8] *Department of Physics and Center for Functional Materials, Wake Forest University, NC 27109, USA*

(Dated: June 14, 2021)

Magnetic Couplings

The magnetic Hamiltonian can be described by three types of couplings: *d*-*d* (between Mn ions), π-π (between BETS dimers), and π-*d* (between Mn and BETS).

$$\begin{aligned}\mathcal{H} = & \sum_{ij} \left(J_{ij}^{\pi\pi}\ \mathbf{s}_i \cdot \mathbf{s}_j + \mathbf{D}_{ij}^{\pi\pi} \cdot \mathbf{s}_i \times \mathbf{s}_j + \mathbf{s}_i \cdot \mathbf{\Gamma}_{ij}^{\pi\pi} \cdot \mathbf{s}_j \right) \\ & + \sum_{in} J_{in}^{\pi d}\ \mathbf{s}_i \cdot \mathbf{S}_n + \sum_{nm} J_{nm}^{dd}\ \mathbf{S}_n \cdot \mathbf{S}_m \\ & + 4 \sum_{ijkl} K_{ijkl}^{\pi\pi} [(\mathbf{s}_i \cdot \mathbf{s}_j)(\mathbf{s}_k \cdot \mathbf{s}_l) \\ & \quad + (\mathbf{s}_j \cdot \mathbf{s}_k)(\mathbf{s}_i \cdot \mathbf{s}_l) - (\mathbf{s}_i \cdot \mathbf{s}_k)(\mathbf{s}_j \cdot \mathbf{s}_l)] \end{aligned} \quad (1)$$

where $\mathbf{s}_i$ is a BETS spin ($S = 1/2$) at site i, $\mathbf{S}_n$ is a Mn spin ($S = 5/2$) at site n. In order to estimate the couplings, we first computed hopping integrals employing two methods: (i) for *d*-*d* and *d*-π hoppings, we employed the full potential local orbital (FPLO) basis [1], generalized gradient approximation (GGA) exchange correlation functional [2] and projective Wannier functions [3]; (ii) for the π-π hoppings we employed ORCA [4] calculations on dimer pairs at the B3LYP/def2-SVP level, using the scheme outlined in [5]. This latter method allows for the incorporation of spin-orbit coupling (SOC) required to address the anisotropic couplings $\mathbf{D}_{ij}^{\pi\pi}$ and $\mathbf{\Gamma}_{ij}^{\pi\pi}$. All calculations were based on the room temperature structure reported in [6]. In this structure, there is disorder in both the positions of the $N(CN)_2$ ligands and ethylene endgroups of the BETS molecules. For the ligands, one out of three dicyanoamine chains has 50% occupancy on each of two positions which are equivalent within $P2_1c$ space group; lowering the space group to $P2_1$ or to P_c is necessary to achive full occupancy; we choose the former. For the ethylene end groups of which every other is disordered, we perform the calculations for the majority (80%) configuration.

We first discuss the *d*-*d* couplings. The Mn atoms form a distorted triangular lattice bridged by dicyanamide ions, with two distinct nearest neighbor bonds having Mn-Mn distances of 7.370 Å and 8.412 Å. The hoppings between Mn *d*-orbitals are presented in Table I. Following Ref. 7, the magnetic couplings can be estimated using:

$$J_{dd} = \frac{4}{25U_d} \sum_{i=1}^{25} t_i^2 \quad (2)$$

where U_d is the average Coulomb repulsion in the *d*-orbitals. Employing $U_d \sim 3-6$ eV, we arrive at:

$$J_{dd}(1) = +0.76 \text{ K to } +1.5 \text{ K} \quad (3)$$

$$J_{dd}(2) = +0.59 \text{ K to } +1.2 \text{ K} \quad (4)$$

These *d*-*d* couplings are both small and geometrically frustrated, which is consistent with the lack of magnetic order in the Mn lattice at measured temperatures.

We next consider the π-*d* couplings. The relevant hoppings are shown in Table II. Following Ref. 7, the magnetic couplings can be estimated using:

$$J_{\pi d} = \frac{4}{5\Delta_{\pi d}} \sum_{i=1}^{5} t_i^2 \quad (5)$$

were $\Delta_{\pi d}$ is the charge transfer energy between the BETS and Mn. Here we approximate $\Delta_{\pi d} \approx U_d$, yielding:

$$J_{\pi d}(1) = +0.04 \text{ K to } +0.08 \text{ K} \quad (6)$$

$$J_{\pi d}(2) = +0.02 \text{ K to } +0.04 \text{ K} \quad (7)$$

$$J_{\pi d}(3) = +0.02 \text{ K to } +0.04 \text{ K} \quad (8)$$

As a result of the large separation of Mn and BETS (and consequently small hopping integrals), the π-*d* couplings are essentially negligible. These results support the experimental findings that the two subsystems

TABLE I. Mn-Mn Hopping parameters (meV) obtained from FPLO.

Mn−Mn (1):		d_{xy}	d_{xz}	d_{yz}	$d_{x^2-y^2}$	d_{z^2}
(7.370 Å)	d_{xy}	+2.4	+2.1	+15.2	~ 0	~ 0
	d_{xz}	+44.2	+0.5	+2.6	~ 0	~ 0
	d_{yz}	-1.6	+0.4	+0.2	~ 0	~ 0
	$d_{x^2-y^2}$	~ 0	~ 0	~ 0	+11.7	+8.3
	d_{z^2}	~ 0	~ 0	~ 0	-6.0	-4.0
Mn−Mn (2):		d_{xy}	d_{xz}	d_{yz}	$d_{x^2-y^2}$	d_{z^2}
(8.412 Å)	d_{xy}	+0.6	+2.2	+1.8	~ 0	~ 0
	d_{xz}	-2.9	-21.0	-0.4	~ 0	~ 0
	d_{yz}	-0.1	-13.6	-15.0	~ 0	~ 0
	$d_{x^2-y^2}$	~ 0	~ 0	~ 0	-0.9	-3.7
	d_{z^2}	~ 0	~ 0	~ 0	-3.5	-31.7

TABLE II. Mn-BETS hopping paramaters (meV) obtained from FPLO.

BETS−Mn (1):		d_{xy}	d_{xz}	d_{yz}	$d_{x^2-y^2}$	d_{z^2}
(9.751 Å)	π MO	-2.3	+1.3	+3.8		
BETS−Mn (2):		d_{xy}	d_{xz}	d_{yz}	$d_{x^2-y^2}$	d_{z^2}
(10.288 Å)	π MO	+1.3	-3.3	-0.2		
BETS−Mn (3):		d_{xy}	d_{xz}	d_{yz}	$d_{x^2-y^2}$	d_{z^2}
(10.731 Å)	π MO	+2.6	+2.0	-0.3		

are essentially decoupled. The computed couplings are orders of magnitude smaller than those estimated for λ-$(BETS)_2FeX_4$ in Ref. 7 following the same method.

To estimate the couplings within the BETS layers, we followed the approach of [5]. In particular, spin-dependent hoppings were computed using ORCA and employed in linked cluster expansion (exact diagonalization) calculations on clusters of up to 4 dimers. For each cluster, the couplings of the low-energy spin Hamiltonian were extracted via projection. For the Coulomb couplings we considered a rescaled version of results from cRPA plus MLWO calculations for ET systems [8], successfully applied in Ref. 5 for various ET compounds. The parameter set consists of an on-site Hubbard repulsion $U = 0.55\,\mathrm{eV}$, on-site Hund's coupling $J_\mathrm{H} = 0.2\,\mathrm{eV}$, and nearest neighbour Hubbard repulsion $V = 0.15\,\mathrm{eV}$. The bilinear π-π magnetic couplings are given in Table III with the generalized bilinear exchange matrix in $\mathcal{H} = \sum_{ij} \mathbf{s}_i \cdot \Lambda_{ij} \cdot \mathbf{s}_j$ defined as:

$$\Lambda_{ij} = \begin{pmatrix} J_{ij} + \Gamma_{ij}^{xx} & \Gamma_{ij}^{xy} + D_{ij}^{z} & \Gamma_{ij}^{xz} - D_{ij}^{y} \\ \Gamma_{ij}^{xy} - D_{ij}^{z} & J_{ij} + \Gamma_{ij}^{yy} & \Gamma_{ij}^{yz} + D_{ij}^{x} \\ \Gamma_{ij}^{xz} + D_{ij}^{y} & \Gamma_{ij}^{yz} - D_{ij}^{x} & J_{ij} - \Gamma_{ij}^{xx} - \Gamma_{ij}^{yy} \end{pmatrix}. \quad (9)$$

The specific orientation of the DM-vectors are depicted in Fig. 1. For a given 4-site plaquette formed by the J-bonds, the DM components in the a^*c direction alternate for each bond, i.e. the total interaction can be written $D_{a^*c}\,(\pm\mathbf{s}_1 \times \mathbf{s}_2 \mp \mathbf{s}_2 \times \mathbf{s}_3 \pm \mathbf{s}_3 \times \mathbf{s}_4 \mp \mathbf{s}_4 \times \mathbf{s}_1)_{a^*c}$. These components lead to a canting in the two-sublattice Néel phase. In the SVC and NCC phase these terms have zero expectation value. In contrast, the b-component takes the same sign for each bond, i.e. $\pm D_b\,(\mathbf{s}_1 \times \mathbf{s}_2 + \mathbf{s}_2 \times \mathbf{s}_3 + \mathbf{s}_3 \times \mathbf{s}_4 + \mathbf{s}_4 \times \mathbf{s}_1)_b = \pm D_b\,[\mathbf{v}_p]_b$. The free energy in the SVC and NCC phase is therefore restricted by symmetry to contain a linear coupling $(0, d_b, 0) \cdot \mathbf{v}$, as presented in Eq. (5) of the main text. Since the order parameter $\mathbf{v}$ is quadratic in spin, the lowest order of coupling to the magnetic field that respects time reversal symmetry is $(\mathbf{h} \cdot \mathbf{v})^2$.

Comparison between ORCA and FPLO

In previous works [5, 9], the application of ORCA to compute the hopping parameters including SOC for ET-salts proved to yield reliable magnetic couplings - particularly the magnitude and orientation of the DM-vector. However, for completeness, we also compare here the ORCA results with isotropic exchange parameters based on the non-relativistic hopping parameters obtained with FPLO. It should be noted that there are several differences in these two approaches: FPLO employs a GGA functional, and includes the full crystalline environment of each molecule, with Wannier functions constructed by projection onto an approximate linear combination of atomic orbitals. In contrast, with ORCA, we have employed a hybrid functional, with Wannier functions constructed via projection onto the precise molecular orbitals of isolated BETS molecules. The latter approach estimates pairwise hoppings from separate calculations on pairs of molecules, and therefore does not account for the full crystalline environment. Despite these major differences, the resulting hoppings are quite similar: from FPLO we estimate: $t_1 = 177$, $t_2 = 8$, $t_3 = 125$, $t_4 = 63$ meV, while ORCA produces: $t_1 = 236$, $t_2 = 19$, $t_3 = 153$, $t_4 = 64$ meV. The hoppings are numbered according to the convention in [10]. The two approaches therefore yield almost the same ratio of $t'/t \sim 0.57$ for FPLO and 0.54 for ORCA. However, all of the hopping integrals from FPLO are smaller by approximately 15 - 20%. To compensate this discrepancy, it is necessary to rescale the two-particle parameters (which had been previously optimized [5] for use in combination with ORCA hoppings) to $U = 0.4$, $J_H = 0.15$, and $V = 0.1$ eV. Then, employing the FPLO hoppings, we estimate $J = 263\,\mathrm{K}$, $J' = 402\,\mathrm{K}$, $J'' = 7.4\,\mathrm{K}$, $J''' = 33\,\mathrm{K}$, $K = 19\,\mathrm{K}$ and $K' = 43\,\mathrm{K}$.

In comparison to the results based on ORCA hoppings, the exchange values are rather similar, with a reduced J'/J ratio and an increased ring-exchange weight K/J and K'/J. Considering the classical state energies given below, these parameters place κ-Mn in the NCC phase,

TABLE III. π-π magnetic couplings (K) between BETS dimers with respect to (a, b, c^*) coordinates.

$\mathcal{J}$:	J	(D_x, D_y, D_z)	$(\Gamma_{xx}, \Gamma_{xy}, \Gamma_{xz}, \Gamma_{yy}, \Gamma_{yz})$
	+260	(+22.6,-1.9,+8.8)	(+0.6,-0.1,+0.4,-0.4,0.0)
$\mathcal{J}'$:	J	(D_x, D_y, D_z)	$(\Gamma_{xx}, \Gamma_{xy}, \Gamma_{xz}, \Gamma_{yy}, \Gamma_{yz})$
	+531	-	-
$\mathcal{J}''$:	J	(D_x, D_y, D_z)	$(\Gamma_{xx}, \Gamma_{xy}, \Gamma_{xz}, \Gamma_{yy}, \Gamma_{yz})$
	+4.7	-	-
$\mathcal{J}'''$:	J	(D_x, D_y, D_z)	$(\Gamma_{xx}, \Gamma_{xy}, \Gamma_{xz}, \Gamma_{yy}, \Gamma_{yz})$
	+25.6	(+2.3,-0.3,+0.9)	(0.1,0.0,0.0,0.0,0.0)

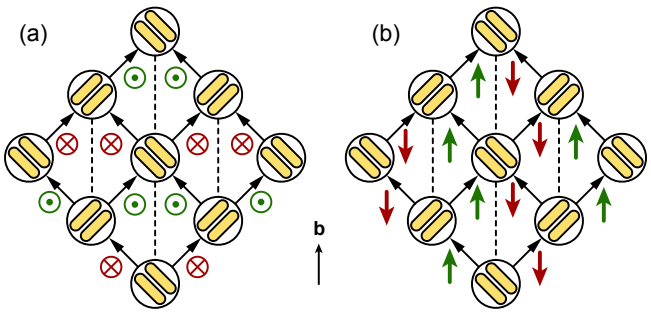

FIG. 1. Orientation of the DM-vectors for each bond, showing (a) the a^*c-component, and (b) the b-axis component. For each bond, the interaction is defined as $\mathbf{D}_{ij} \cdot (\mathbf{s}_i \times \mathbf{s}_j)$, with the black arrow pointing from site i to site j. The b-axis component has same periodicity as a staggered vector-chirality.

with a relatively small out-of-plane tilting angle $\theta = 15°$. This phase still has a large staggered vector chirality with $\mathbf{v}||b$, and thus would respond similarly in the magnetic torque to the SVC phase. In the ^{13}C NMR, we would expect additional peaks to appear due to the reduction of symmetry, but these may be buried within the experimental linewidth. Therefore, although we find no specific evidence for finite out-of-plane moments, their possibility should not be completely ruled out.

Classical State Energies

In this section, we give the analytical expressions for the ground state energies (per site) for the classical states discussed in the main text (valid for antiferromagnetic signs of all J couplings). These states are depicted in Fig. 2.

First, we consider the orders identified in [11]. At small K, the ground states are the colinear two-sublattice "(π, π)" Néel order, and "(q, q)" spiral. The energies as a function of q can be summarized by:

$$\frac{E}{S^2} = 2J\cos(q) + J'\cos(2q) + J'' + 2J'''\cos(3q) + K + 2K' \tag{10}$$

where the ordering wavevector is given in the Brillouin zone of the primitive cell of the square lattice. Within the Néel phase, the minimum energy is obtained for $q = \pi$, yielding:

$$\frac{E_{\text{2SL}}}{S^2} = -2J + J' + J'' - 2J''' + K + 2K' \tag{11}$$

Within the spiral phase, the minimum energy q-vector is given by:

$$q = \cos^{-1}\left(\frac{J_c - J'}{12J'''}\right) \tag{12}$$

where:

$$J_c = \sqrt{(J')^2 - 12JJ''' + 36(J''')^2} \tag{13}$$

which yields:

$$\frac{E_{\text{sp}}}{S^2} = J'' - \frac{J'}{2} + K + 2K' + \frac{(J')^3 - 18JJ'J''' - J_c^3}{108(J''')^2} \tag{14}$$

At large K, there are three competitive states. The first is the two-sublattice collinear "$(\pi, 0)$" stripe order, with energy:

$$\frac{E_{(\pi,0)}}{S^2} = -J' - J'' + K + 2K'; \tag{15}$$

The chiral states have energy:

$$\frac{E}{S^2} = -J - J''' + \frac{K}{4} + K' + (J - J' + J''' - J'' - K)\cos(2\theta) + \left(K' - \frac{K}{4}\right)\cos(4\theta) \tag{16}$$

where $0 \le \theta \le \frac{\pi}{2}$ is the angle of tilting of the spins out of the plane. The Néel state is recovered by taking $\theta = \frac{\pi}{2}$. In the coplanar vector chiral spin-vortex crystal (SVC), $\theta = 0$. The energy is:

$$\frac{E_{\text{SVC}}}{S^2} = -J' - J'' - K + 2K' \tag{17}$$

The SVC may be viewed as a multi-q order that is a linear combination of $(\pi, 0)$ and $(0, \pi)$ stripes. Classically, the SVC state is strictly lower in energy than the $(\pi, 0)$ single-stripe phase for $K > 0$. As a result, we do not find any region where the single-stripe phase represents the classical ground state. Finally, the four-sublattice non-coplanar chiral (NCC) order corresponds to the region of intermediate θ values. Assuming $\text{sign}(J_a - J_b) = \text{sign}(K - 4K')$, the tilting angle can be expressed as:

$$2\theta = \cos^{-1}\left(\frac{J_a - J_b}{K - 4K'}\right) \tag{18}$$

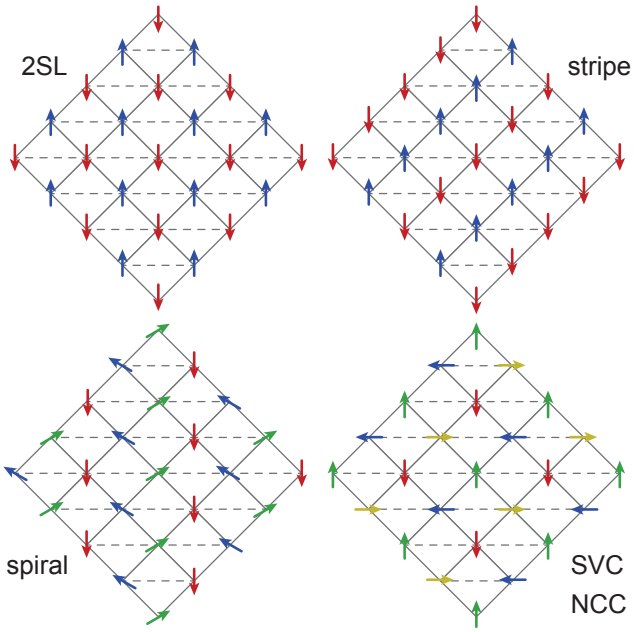

FIG. 2. Ordering patterns for the classical ground states mentioned in the text.

where:

$$J_a = J + J''' \tag{19}$$
$$J_b = J' + J'' \tag{20}$$

This yields:

$$\frac{E_{\rm NCC}}{S^2} = \frac{\frac{1}{2}(J_a - J_b)^2 + KJ_b + (K - 2J_a)(K - 2K')}{K - 4K'} \tag{21}$$

^{13}C NMR Hyperfine Tensors

In order to analyse the ^{13}C NMR results, we first estimated the hyperfine coupling tensors for isolated $[BETS_2]^{1+}$ dimers via *ab initio* calculations using ORCA [4] at the B3LYP/EPR-II/def2-SVP level. Each dimer contains four ^{13}C sites, with pairs of sites being related by inversion symmetry. As a result, there are two unique sites per dimer, conventionally labelled "inner" and "outer" (see [12]). Further, there are two dimers per unit cell (sublattice A and B), related by 2_1 screw axis. The computed hyperfine tensors (units kOe/μ_B), in the crystallographic (a^*, b, c) coordinate system are:

$$\text{Dimer A, Outer:}\quad \mathbb{A}_{\rm out} = \begin{pmatrix} +0.9 & +2.6 & -1.6 \\ +2.6 & +8.8 & -6.4 \\ -1.6 & -6.4 & +4.1 \end{pmatrix} \tag{22}$$

$$\text{Dimer A, Inner:}\quad \mathbb{A}_{\rm in} = \begin{pmatrix} -2.2 & +0.8 & -0.4 \\ +0.8 & +2.0 & -4.2 \\ -0.4 & -4.2 & +0.4 \end{pmatrix} \tag{23}$$

$$\text{Dimer B, Outer:}\quad \mathbb{A}_{\rm out} = \begin{pmatrix} +0.9 & -2.6 & -1.6 \\ -2.6 & +8.8 & +6.4 \\ -1.6 & +6.4 & +4.1 \end{pmatrix} \tag{24}$$

$$\text{Dimer B, Inner:}\quad \mathbb{A}_{\rm in} = \begin{pmatrix} -2.2 & -0.8 & -0.4 \\ -0.8 & +2.0 & +4.2 \\ -0.4 & +4.2 & +0.4 \end{pmatrix} \tag{25}$$

The computed tensors may be validated by comparison with experimentally derived values for various ET salts [12–15]. To facilitate this comparison, we rotate the computed tensors into the molecular coordinates of Ref. 12 and 15: the x_m-axis is taken to be parallel to the central C-C bond, and the y_m-axis is the perpendicular direction within the molecular plane. In these coordinates, we find:

$$\mathbb{A}_{\rm out} = \begin{pmatrix} 0.2 & 0.0 & -0.6 \\ 0.0 & -0.4 & -0.1 \\ -0.6 & -0.1 & +15.1 \end{pmatrix} \tag{26}$$

$$\mathbb{A}_{\rm in} = \begin{pmatrix} -2.3 & +0.0 & +0.9 \\ +0.0 & -3.3 & +0.3 \\ +0.9 & +0.3 & +6.0 \end{pmatrix} \tag{27}$$

Not surprisingly, the hyperfine tensor is dominated by the $[\mathbb{A}]_{zz}$ component, as the unpaired electrons occupy π-orbitals with p_z character in the molecular coordinate system [12]. Further, we find that $[\mathbb{A}_{\rm out}]_{zz} > [\mathbb{A}_{\rm in}]_{zz}$, consistent with the experimental trends for ET salts. The absolute magnitudes of the principle components are also consistent with those reported in [13, 14]. We therefore conclude that the estimated hyperfine tensors are of sufficient accuracy to simulate the experimental NMR spectra.

Specific Heat Measurements

Experimental Details - Measurements of specific heat were performed by employing a high-resolution ac-modulation technique [16] on a single crystal of mass $m = (40 \pm 20)\,\mu$g. Details of the setup, specially designed for measuring very small plate-like crystals, such as κ-Mn, are presented in [17]. Measurements were performed upon warming in the temperature range $1.8\,{\rm K} \leq T \leq 29\,{\rm K}$. For the measurements, the temperature oscillation amplitude ΔT at each temperature T was typically

chosen such that $\Delta T \sim 0.01\,T$. The finite oscillation amplitude in the ac-modulation technique typically causes that the specific heat feature of sharp first-order transitions, as is the case for the MI transition in κ-Mn, are slightly broadened.

Background subtraction - The specific heat of κ-Mn is dominated by phononic contributions, as is evident from the measured data shown in the insets in Fig. 3. Unfortunately, a non-magnetic reference material is not available for an independent determination of the phononic background. This renders a precise determination of associated entropies difficult. Nevertheless, our data can be used to obtain estimates of the entropies associated with the Mn and BETS ordering.

To this end, we obtained the anomalous contribution to the specific heat by modelling the background with a phononic contribution, $C_{v,\mathrm{ph}}$. Below the MIT at T_N, there is no charge contribution to the specific heat in κ-Mn ($\gamma = 0$). Above T_N, the charge contribution is finite, but likely very small compared to the phononic contribution for high T. Based on typical γ values of organic charge-transfer salts [18], we can estimate $C_{v,\mathrm{el}} = \gamma T \sim 600\,\mathrm{mJ{\cdot}mol^{-1}{\cdot}K^{-1}} \ll C_{v,\mathrm{ph}}$. As a result, we neglect electronic contributions in our background modelling. For organic charge-transfer salts it has often been reported that the low-temperature specific heat is dominated by Debye and Einstein contributions, resulting from acoustical and low-lying optical phonons [19]. In order to keep the number of fitting parameters small, we considered only one Einstein and one Debye temperature. Thus, we employed following Einstein-Debye form to model $C_{v,\mathrm{ph}}$:

$$C_{v,\mathrm{ph}} = 9k_B n_D \left(\frac{T}{\Theta_D}\right)^3 \int_0^{\frac{\Theta_D}{T}} dx\ \frac{x^4 e^x}{(e^x-1)^2} + 3k_B n_E \left(\frac{\Theta_E}{T}\right)^2 \frac{e^{\Theta_E/T}}{(e^{\Theta_E/T}-1)^2} \qquad (28)$$

where T is the temperature, k_B is the Boltzmann constant, Θ_D is the Debye temperature, and Θ_E is the Einstein temperature. The number of phonon modes of Debye and Einstein type are given by $3n_D$ and $3n_E$, respectively, where we constrain $(n_D + n_E)/N_A = 68$, the total number of atoms per formula unit. We note that we included a scaling factor in our model in order to account for errors in the determination of the very small mass of the crystal as well as for potential errors resulting from the subtraction of addenda contributions. Given that there are huge magnetic contributions to the specific heat at low temperatures due to the Mn spins, we had to exclude the data at very low temperatures from the fit. Instead, we performed fits across different windows at intermediate temperatures below, but close to T_N. In addition, we included the specific heat data for $T \geq 24\,\mathrm{K}$ (i.e., $T > T_\mathrm{N}$) in each fit, since we expect this data to be largely dominated by phononic contributions.

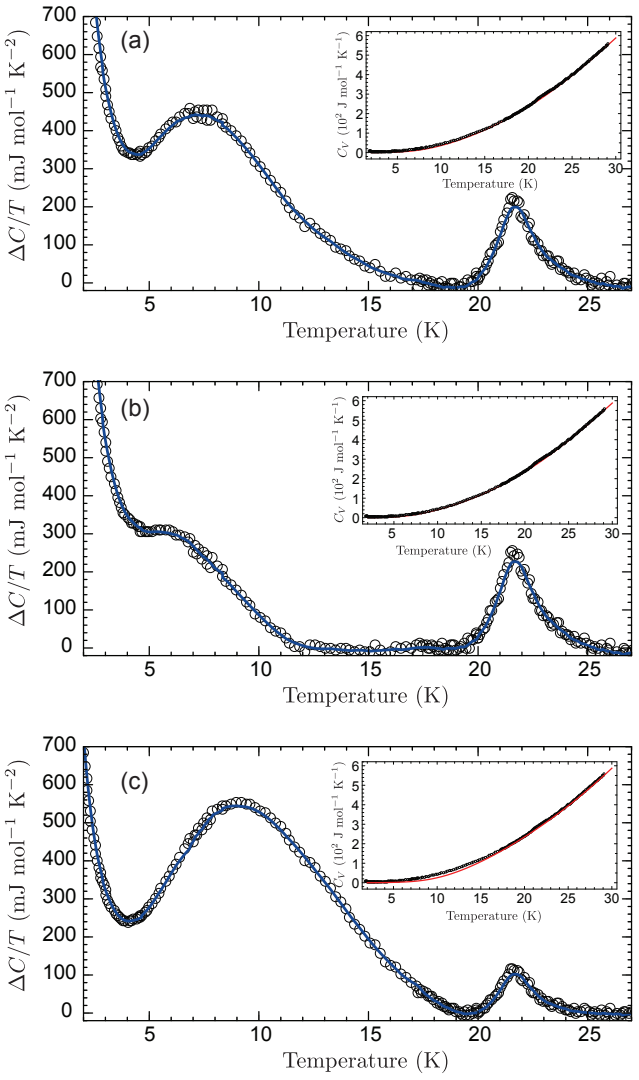

FIG. 3. Comparison of different background modelling for the specific heat data. In each panel (a)-(c), we show $\Delta C/T$ curves which were obtained after subtraction of different phononic background model curves. The insets in each panel show the measured raw data (open blue symbols) and the background fit (red line) that was used to obtain $\Delta C/T$ in the respective main panel. The fitting range and the fitting parameters are discussed in the text.

In Fig. 3 we compare the results of different background fits. In (a) we show the fit that was used in the main text. This fit (see red line in the inset) was obtained by simultaneously fitting the experimental specific heat (see open symbols in the inset) in the ranges $16\,\mathrm{K} \leq T \leq 19\,\mathrm{K}$ and $T \geq 24\,\mathrm{K}$. The fit parameters were $n_E = 1.8 \times 10^{24}\,\mathrm{mol^{-1}}$, $\Theta_E = (55 \pm 4)$ K, and $\Theta_D = (219 \pm 6)$ K. The values of Θ_D and Θ_E are well consistent with values typically observed in organic charge-transfer salts. Θ_D values typically range from 180 K to 220 K [20–23]. Θ_E values have been re-

ported to be $\sim 28\,\mathrm{K}$ for κ-$(ET)_2I_3$ [20] or $\sim 46\,\mathrm{K}$ for κ-$(ET)_2Hg(SCN)_2Cl$ [24]. Thus, we infer that this modeling of the phononic background contribution for κ-Mn is reasonable.

For comparison, we show in (b) and (c) other fits, where the lower-T fitting range was varied to a larger window [$11\,\mathrm{K} \leq T \leq 19\,\mathrm{K}$ (b)] and a smaller window [$19\,\mathrm{K} \leq T \leq 20\,\mathrm{K}$ (c)]. As we will discuss now, the choice of fitting window primarily affects the amount of entropy assigned to the Mn features below T_N.

The fit in (b) yielded $\Theta_D = (209 \pm 2)\,\mathrm{K}$, $\Theta_E = (47 \pm 3)\,\mathrm{K}$ and $n_E = 1.3 \times 10^{24}$ mol^{-1}, which are similar to the values of the fit in (a). The entropies that can be inferred from this fit amount to $\Delta S_\mathrm{Mn} = \int_2^{19} \Delta C/T \; dT \approx 2.7$ J mol^{-1} K^{-1} for the Mn correlations and $\Delta S_\mathrm{MIT} = \int_2^{19} \Delta C/T \; dT \approx 0.5\,\mathrm{J}$ mol^{-1} K^{-1} for the BETS ordering. Thus, shifting the fitting window does not result in a significantly different estimate of ΔS_MIT, but reduces the estimate of ΔS_Mn. The latter is not surprising, since the extended fitting window cuts off large amounts of the low T entropy. Nevertheless, the low-T entropy is so large that it is only reasonable to associate it with the Mn spins.

Finally, the fit in (c) resulted in $\Theta_D = (293 \pm 47)\,\mathrm{K}$, $\Theta_E = (74 \pm 3)\,\mathrm{K}$, which are clearly out of the range of reported values for organic charge-transfer salts, and $n_E = 2.7 \times 10^{24}$ mol^{-1}. Given the small range of fitting, this phononic model can be expected to be the least accurate. Nonetheless, similar entropy estimates of $\Delta S_\mathrm{Mn} = \int_2^{19} \Delta C/T \; dT \approx 5.511$ J mol^{-1}K^{-1} and $\Delta S_\mathrm{MIT} = \int_{19}^{25} \Delta C/T \; dT \approx 0.202$ J mol^{-1} K^{-1} were obtained. Thus, the conclusion that the entropy change at T_N is far too small to indicate significant coupling between the Mn and BETS spins remains robust against the broad details of the phononic background model.

Independent crosscheck of ΔS_MIT - In order to confirm our entropy estimate ΔS_MIT independently, we also calculated the entropy from the Clausius-Clapeyron equation using data of the thermal expansion [25] and the published pressure dependence of T_N [26]. This analysis yielded $\Delta S_\mathrm{MIT} \sim 0.4\,\mathrm{J{\cdot}mol^{-1}{\cdot}K^{-1}}$ which is consistent with the value inferred from specific heat in the main text. This not only confirms that our background determination of the specific heat is solid, but also that the entropy change across the MIT transition is too small for Mn atoms to be significantly involved.

[1] K. Koepernik and H. Eschrig, Phys. Rev. B **59**, 1743 (1999).
[2] J. P. Perdew, K. Burke, and M. Ernzerhof, Phys. Rev. Lett. **77**, 3865 (1996).
[3] H. Eschrig and K. Koepernik, Phys. Rev. B **80**, 104503 (2009).
[4] F. Neese, F. Wennmohs, U. Becker, and C. Riplinger, J. Chem. Phys. **152**, 224108 (2020).
[5] S. M. Winter, K. Riedl, and R. Valentí, Phys. Rev. B **95**, 060404(R) (2017).
[6] N. D. Kushch, E. B. Yagubskii, M. V. Kartsovnik, L. I. Buravov, A. D. Dubrovskii, A. N. Chekhlov, and W. Biberacher, J. Am. Chem. Soc. **130**, 7238 (2008).
[7] T. Mori and M. Katsuhara, J. Phys. Soc. Japan **71**, 826 (2002).
[8] K. Nakamura, Y. Yoshimoto, and M. Imada, Phys. Rev. B **86**, 205117 (2012).
[9] K. Riedl, R. Valentí, and S. M. Winter, Nat. Commun. **10**, 2561 (2019).
[10] D. Guterding, R. Valentí, and H. O. Jeschke, Phys. Rev. B **92**, 081109 (2015).
[11] M. Holt, B. J. Powell, and J. Merino, Phys. Rev. B **89**, 174415 (2014).
[12] K. Miyagawa, K. Kanoda, and A. Kawamoto, Chem. Rev. **104**, 5635 (2004).
[13] H. Mayaffre, P. Wzietek, C. Lenoir, D. Jérome, and P. Batail, EPL (Europhysics Letters) **28**, 205 (1994).
[14] S. M. De Soto, C. P. Slichter, A. M. Kini, H. Wang, U. Geiser, and J. Williams, Phys. Rev. B **52**, 10364 (1995).
[15] Y. Saito and A. Kawamoto, Solid State Nucl. Magn. Reson. **73**, 22 (2016).
[16] P. F. Sullivan and G. Seidel, Phys. Rev. **173**, 679 (1968).
[17] J. Müller, M. Lang, R. Helfrich, F. Steglich, and T. Sasaki, Phys. Rev. B **65**, 140509 (2002).
[18] Y. Nakazawa and K. Kanoda, Phys. Rev. B **53**, R8875 (1996).
[19] R. Świetlik, H. Grimm, D. Schweitzer, and H. J. Keller, Z. Naturforsch. A **42**, 603 (1987).
[20] J. Wosnitza, X. Liu, D. Schweitzer, and H. J. Keller, Phys. Rev. B **50**, 12747 (1994).
[21] S. Katsumoto, S.-i. Kobayashi, H. Urayama, H. Yamochi, and G. Saito, J. Phys. Soc. Japan **57**, 3672 (1988).
[22] B. Andraka, J. S. Kim, G. R. Stewart, K. D. Carlson, H. H. Wang, and J. M. Williams, Phys. Rev. B **40**, 11345 (1989).
[23] G. R. Stewart, J. O'Rourke, G. W. Crabtree, K. D. Carlson, H. H. Wang, J. M. Williams, F. Gross, and K. Andres, Phys. Rev. B **33**, 2046 (1986).
[24] E. Gati, J. K. H. Fischer, P. Lunkenheimer, D. Zielke, S. Köhler, F. Kolb, H. A. K. von Nidda, S. M. Winter, H. Schubert, J. A. Schlueter, H. O. Jeschke, R. Valentí, and M. Lang, Phys. Rev. Lett. **120**, 247601 (2018).
[25] Y. Agarmani, T. Thomas, S. Hartmann, M. Kartsovnik, N. Kushch, S. Winter, M. Lang, and J. Müller, in preparation.
[26] V. N. Zverev, M. V. Kartsovnik, W. Biberacher, S. S. Khasanov, R. P. Shibaeva, L. Ouahab, L. Toupet, N. D. Kushch, E. B. Yagubskii, and E. Canadell, Phys. Rev. B **82**, 155123 (2010).